ACS Catalysis

Research Article

pubs.acs.org/acscatalysis

Active Sites and Structure–Activity Relationships of Copper-Based Catalysts for Carbon Dioxide Hydrogenation to Methanol

Sittichai Natesakhawat,*[,†,‡] Jonathan W. Lekse,[†] John P. Baltrus,[†] Paul R. Ohodnicki, Jr.,[†] Bret H. Howard,[†] Xingyi Deng,[†,§] and Christopher Matranga[†]

[†]National Energy Technology Laboratory, United States Department of Energy, P.O. Box 10940, Pittsburgh, Pennsylvania 15236, United States

[‡]Department of Chemical and Petroleum Engineering, University of Pittsburgh, Pittsburgh, Pennsylvania 15260, United States

[§]URS, P.O. Box 618, South Park, Pennsylvania 15129, United States

Supporting Information

ABSTRACT: Active sites and structure–activity relationships for methanol synthesis from a stoichiometric mixture of CO_2 and H_2 were investigated for a series of coprecipitated Cu-based catalysts with temperature-programmed reduction (TPR), X-ray diffraction (XRD), transmission electron microscopy (TEM), X-ray photoelectron spectroscopy (XPS), and N_2O decomposition. Experiments in a reaction chamber attached to an XPS instrument show that metallic Cu exists on the surface of both reduced and spent catalysts and there is no evidence of monovalent Cu^+ species. This finding provides reassurance regarding the active oxidation state of Cu in methanol synthesis catalysts because it is observed with 6 compositions possessing different metal oxide additives, Cu particle sizes, and varying degrees of ZnO crystallinity. Smaller Cu particles demonstrate larger turnover frequencies (TOF) for methanol formation, confirming the structure sensitivity of this reaction. No correlation between TOF and lattice strain in Cu crystallites is observed suggesting this structural parameter is not responsible for the activity. Moreover, changes in the observed rates may be ascribed to relative distribution of different Cu facets as more open and low-index surfaces are present on the catalysts containing small Cu particles and amorphous or well-dispersed ZnO. In general, the activity of these systems results from large Cu surface area, high Cu dispersion, and synergistic interactions between Cu and metal oxide support components, illustrating that these are key parameters for developing fundamental mechanistic insight into the performance of Cu-based methanol synthesis catalysts.

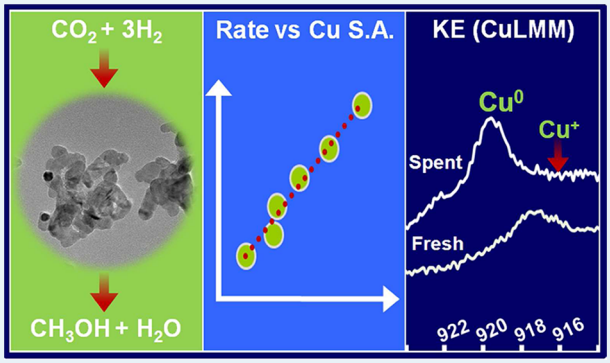

KEYWORDS: *methanol, carbon dioxide, hydrogenation, copper, gallium, yttrium, active sites, strain*

INTRODUCTION

Technologies developed for utilizing carbon dioxide as a reactant to produce useful products offer opportunities to mitigate CO_2 emissions while generating revenues to offset the costs associated with carbon management. An optimal solution is to convert CO_2 into commodity chemicals with large demand, which can be utilized within the infrastructure already existing in end-use sectors.[1] Thermocatalytic hydrogenation of CO_2 ($CO_2 + 3H_2 \rightarrow CH_3OH + H_2O$) is a viable option because methanol is produced in large quantities rather than ppm levels. Methanol can be directly utilized as a fuel or further converted into many industrial chemicals such as acetic acid, formaldehyde, and dimethyl terephthalate. This process can be driven by a variety of renewable and carbon friendly energy sources such as solar, wind, and industrial waste heat, thus making the chemical recycling of CO_2 into fuels and chemicals a reality.[2]

Currently, commercial synthesis of methanol is accomplished by hydrogenation of syngas containing small amounts of CO_2 (e.g., less than 6 volume%) over coprecipitated $Cu/ZnO/Al_2O_3$ catalysts at 230–240 °C and 40–100 bar.[3] The low activity and stability of existing formulations, which is partly attributed to Cu sintering accelerated by the presence of water vapor byproduct, create major barriers toward using them in realistic CO_2-rich conditions. Cu/ZnO catalysts containing zirconia instead of alumina have demonstrated high performance in methanol synthesis from CO_2 because of the high thermal stability of zirconia under reducing and oxidizing atmospheres.[4−13] To further improve the performance of these catalytic systems, an effective promoter is needed to achieve larger Cu surface area, higher Cu dispersion, and easier reduction of CuO to metallic Cu. Among all the promoters investigated, Ga_2O_3 has emerged as a promising candidate.[7,14−18] Y_2O_3 is another useful additive because it is capable

Received: January 6, 2012
Revised: June 21, 2012
Published: June 21, 2012

Table 1. Bulk Compositions and BET Surface Areas of the Catalysts Calcined at 350 °C

	metal content (mol %)[a]					
catalyst	Cu	Zn	Zr	Ga	Y	BET surface area (m^2/g)
CuO	100 (ND)[b]					21
ZnO		100 (ND)[b]				40
CuZr	40 (52)		60 (48)			157
CuZn	40 (41)	60 (59)				65
CuZnZr	40 (45)	30 (31)	30 (24)			126
CuZnZrGa	35 (39)	26 (29)	26 (21)	13 (11)		143
CuZnZrY	35 (37)	26 (27)	26 (21)		13 (15)	96
CuZnZrGaY	31 (35)	23 (24)	23 (19)	11.5 (9)	11.5 (13)	125

[a]The numbers in parentheses are actual metal contents determined by ICP-OES. [b]ND = not determined.

of maintaining high copper surface area during the steam reforming of methanol.[19] Furthermore, Y_2O_3 is commonly used for stabilizing the crystal structure of ZrO_2 in yttria-stabilized zirconia (YSZ), which is an electrolyte for solid oxide fuel cells. Surprisingly, the use of yttria as a promoter for methanol synthesis catalysts is very scarce.

Despite extensive studies of methanol synthesis over Cu-based catalysts, there is still no consensus on the nature of active sites in these materials. Metallic Cu is believed to be an active phase because the activity was found to be proportional to Cu surface area.[20−24] However, other researchers were not able to establish a linear activity-Cu surface area relationship and suggested that a synergy between copper and the oxide components in the catalysts also influenced activity.[4,25,26] Both Cu^0 and Cu^+ species were believed to contribute to the activity of Cu-based catalysts and Zn-deposited Cu(111) model catalysts as indicated by the volcano-shaped dependence of activity on the oxygen coverage of the Cu surface.[27,28] Other factors which have been suggested to influence activity include Cu^+ dissolved in ZnO,[29,30] Cu steps decorated with Zn atoms,[31] the formation of Cu−Zn surface alloys,[32−34] and the presence of Cu-ZnO interfacial sites.[35−38] Additional structural aspects of the catalysts such as lattice strain,[39,40] and crystal phase of the support[41] have also been hypothesized to play a role in activity. As such, the true role of Cu^0 and Cu^+ species, support effects, and the structure−activity relationships for CO_2 hydrogenation catalysts are not fully understood. Therefore, a better understanding of active sites and structure−activity relationships is essential for the rational design of new catalysts that would be suitable for CO_2 conversion applications.

In this paper, Cu-based catalysts were synthesized by a reverse coprecipitation technique and were evaluated for methanol synthesis under the stoichiometric condition (i.e., $H_2/CO_2 = 3$). The catalyst compositions were carefully chosen from our separate optimization study by systematically varying the Cu/metal molar ratios. Gallium and yttrium oxides were used as promoters since they have been shown to improve Cu surface area and dispersion allowing a reasonable level of control over particle size. By using different compositions of gallium, yttrium, zinc, and zirconium for the metal oxide additives, we were able to investigate the role of Cu surface area and lattice strain on catalytic activity. The incorporation of Ga_2O_3 and Y_2O_3 into our catalyst formulations also suppresses the crystallization of ZnO during heat treatment, resulting in well-dispersed or amorphous ZnO undetectable by X-ray diffraction (XRD). We employed N_2O decomposition and Rietveld refinements of in situ X-ray diffraction patterns to determine Cu crystallite size, and there is a very good agreement between these two methods. Overall, we were able to demonstrate that the active state of copper is Cu^0 with no spectroscopic evidence for the participation of Cu^+ species. The dependence of turnover frequency on Cu crystallite size indicates that the CO_2 hydrogenation to methanol reaction over Cu-based catalysts is structure-sensitive. The activity is not proportional to lattice strain suggesting that it is not the main structural parameter responsible for the activity of the systems examined in this study. An increase in rates with smaller crystallites may be attributed to larger numbers of open planes, edge/defect sites containing coordinately unsaturated atoms which are strongly bound to critical reactive intermediates. This finding further suggests that open Cu facets are a more accurate model for active sites in real catalysts and that support effects through a synergy between Cu and ZnO cannot be neglected. As such, future experiments and computational modeling should focus on investigating these parameters to improve the performance of these materials for converting CO_2 to methanol and to better understand the reaction mechanisms.

EXPERIMENTAL SECTION

Catalyst Synthesis. Catalysts were prepared by a reverse coprecipitation method similar to that described in detail elsewhere.[10] All metal precursors (Aldrich) used were in a nitrate form. $NaHCO_3$ (0.1 M) was used as a precipitating agent. The Cu content of the binary and ternary catalysts was chosen at 40 mol % because it was an optimum value with respect to the catalytic performance.[21,42] The Cu/Zn and Cu/Zr molar ratios of the ternary and multicomponent catalysts were kept constant at 1.3. Initially, aqueous metal nitrate solutions were prepared and mixed in a beaker with appropriate ratios to yield the desired composition as indicated in Table 1. The resulting mixture was then added dropwise into 500 cm^3 of 0.1 M $NaHCO_3$ which was stirred vigorously in an ultrasonic bath at room temperature. The pH of the mixture was maintained around 7 throughout the synthesis by adding a separate portion of 0.1 M $NaHCO_3$ dropwise. The suspension was stirred and ultrasonicated for an additional 30 min and was subsequently aged for 2 h. The mother liquor was discarded, and the remaining precipitate left at the bottom of the beaker was washed with 2 L of hot deionized water to remove residual sodium. The washed precipitate was dried in an oven at 110 °C overnight. Dried samples were ground to a fine powder and were calcined in flowing air by ramping at 5 °C/min to 350 °C and holding for 4 h.

Catalyst Characterization. Brunauer−Emmett−Teller (BET) surface areas of freshly calcined catalysts were measured by N_2 adsorption at 77 K and relative pressures (P/P_0) in the range of 0.1−0.3 using a Quantachrome Autosorb 1-C. Before measurements, samples were degassed under vacuum at 110 °C

dx.doi.org/10.1021/cs300008g | ACS Catal. 2012, 2, 1667−1676

overnight. The BET surface areas of the catalysts prepared in this study are listed in Table 1. The chemical compositions of the calcined catalysts were determined by Inductively Coupled Plasma-Optical Emission Spectroscopy (ICP-OES) using a Perkin-Elmer Optima 3000 (Table 1). Prior to analysis, samples were dissolved in hydrochloric acid, microwaved, and then diluted with deionized water to provide the analytical solutions.

Copper surface area and dispersion were measured by a nitrous oxide decomposition method using a Micromeritics Autochem 2950 HP. The catalysts (100 mg) were first reduced with 10% H_2/Ar at 250 °C for 2 h followed by purging with He for 30 min and cooling to 60 °C. The catalysts were then exposed to 10% N_2O/He for 1 h to oxidize surface copper atoms to Cu_2O, and the decomposition of N_2O to N_2 was monitored using a Pfeiffer Vacuum Thermostar mass spectrometer. The samples were cooled to room temperature, and temperature-programmed reduction (TPR) was performed under a 10% H_2/Ar flow to reduce Cu_2O back to metallic Cu using a ramp rate of 10 °C/min to 300 °C. Copper surface area and dispersion were calculated from the amount of H_2 consumed during the TPR step by assuming that copper crystallites are spherical.[43,44] Equation 1 is used to calculate Cu surface area.

$$\text{Cu S.A. } (m^2/g_{Cu}) = [100(\text{Mol } H_2)(SF)(N_A)] / [(SD_{Cu})(W_{Cu})] \quad (1)$$

where Mol H_2 = amount of H_2 consumed during the TPR step per unit mass of the catalyst (mol H_2/g_{cat}), SF = stoichiometric factor =2, N_A = Avogadro's number = 6.022×10^{23} atoms/mol, SD_{Cu} = copper surface density =1.47×10^{19} atoms/m^2, W_{Cu} = Cu content of the catalyst determined from elemental analysis (wt %).

Copper dispersion is defined as the ratio of the surface copper atoms to the total copper atoms present in the catalyst.[3,45] Equation 2 is used to calculate % Cu dispersion from the same experiment.

$$\%D_{Cu} = [10^4(\text{Mol } H_2)(SF)(\text{At.Wt.}_{Cu})]/W_{Cu}) \quad (2)$$

where At.Wt._{Cu} = Atomic weight of Cu = 63.54.

Additional TPR experiments were also conducted separately to examine the catalyst reducibility. Initially, 50 mg of the catalyst was heated in He at 350 °C for 30 min, followed by cooling to room temperature. The catalyst temperature was then raised in 50 cm^3(STP)/min of 10% H_2/Ar using a ramp rate of 10 °C/min to 500 °C. The effluent from the reactor was passed through a trap immersed in an isopropyl alcohol/liquid nitrogen bath to remove moisture formed during reduction. H_2 consumption was detected using a thermal conductivity detector (TCD).

X-ray powder diffraction (XRD) patterns of both calcined and reduced catalysts were obtained with a PANalytical X'Pert Pro MPD diffractometer using Cu K_α radiation (λ = 1.542 Å) operated at 45 kV and 40 mA. In situ reduction was performed with a computer-controlled Anton Parr hot stage in flowing 4% H_2/N_2 (15 cm^3(STP)/min) by ramping at 10 °C/min to 250 °C followed by an isothermal soak for 2 h. Following reduction, the patterns of a standard reference material (NIST 640B silicon) and the catalysts were then collected from 20° to 138° with a scanning rate of 0.12°/min. Determination of copper crystallite size and microstrain from Rietveld refinements was performed by fitting the peaks in the XRD patterns using the pseudo-Voigt function (PVF) in X'Pert Highscore Plus software (See Supporting Information). Patterns of spent catalysts collected from the reactor after 12 h-testing at 240 °C and 20 bar were also obtained.

Transmission electron microscopy (TEM) images and selected area diffraction patterns were obtained with a JEOL 2000 microscope. The catalysts collected from the XRD sample holder after reduction at 250 °C were ultrasonically dispersed in ethanol, and a few drops of the suspension were deposited on Si-nitride grids purchased from Ted-Pella, Inc. X-ray photoelectron spectroscopy (XPS) was performed using a PHI 5600ci instrument equipped with a monochromatic Al X-ray source ($h\nu$ = 1486.6 eV) operated at 400 W. The pass energy of the analyzer was set at 58.7 eV. Treatments of the catalysts were conducted by transferring the samples under ultrahigh vacuum to a separate 30-cm^3 reaction chamber that was attached directly to the XPS chamber. The calcined samples were first analyzed and then transferred under vacuum to the reaction chamber, exposed to a 10% H_2/Ar flow of 50 cm^3(STP)/min at 250 °C for 2 h, cooled to room temperature, and evacuated. The samples were then transferred back to the analysis chamber without exposure to air. After the data collection was completed, the reduced catalysts were moved back to the reaction chamber and were exposed to a 25% CO_2/H_2 flow of 50 cm^3(STP)/min at 240 °C for 8 h. The corresponding CO_2 and H_2 partial pressures were 190 and 570 Torr, respectively. Finally, they were again transferred back to the analysis chamber for acquiring post-reaction spectra. Peak binding energies were referenced to the Zn $2p_{3/2}$ peak located at 1021.1 eV.

CO_2+H_2-temperature-programmed reaction (CO_2+H_2-TPReaction) was also carried out with the Micromeritics Autochem 2950 HP to verify that the working catalysts were characterized by XPS. The feed gas (25% CO_2/H_2, 50 cm^3(STP)/min) was introduced to the reduced catalysts while the reactor was kept at atmospheric pressure. The catalyst temperature was raised linearly at the rate of 10 °C/min from room temperature to 350 °C. Fragments of the gas components in the outlet stream of the reactor, for example, CO_2 (m/z = 44), CH_3OH (m/z = 31), CO (m/z = 28), and H_2O (m/z = 18) were monitored using a Thermostar mass spectrometer.

Activity Measurements. Steady-state reaction experiments were performed using a fixed-bed flow reactor system (Process Integral Development Engineered & Tech., Spain) with a stainless steel tubular reactor (ID = 9.2 mm, L = 300 mm). The prepared catalysts were evaluated at 240 °C and 20 bar. The feed composition was $CO_2/H_2/N_2$ = 1/3/0.4 (total flow rate = 100 cm^3(STP)/min). The weight hourly space velocity (WHSV) was maintained at 0.03 m^3/g_{cat}/h to ensure that the reaction conditions did not allow the system to approach the equilibrium-limited regime. Prior to reaction, the catalysts were reduced in situ with 10% H_2/N_2 (50 cm^3(STP)/min) at 250 °C and atmospheric pressure for 2 h. The feed and effluent streams were analyzed online using an automated Agilent GC 7890A equipped with FID and TCD detectors and a methanizer. Separation of components was performed using Ar as a carrier gas and 2 columns: Hayesep Q (10 ft × 1/8 in. SS, 80/100 mesh) and molecular sieve 13X (6 ft × 1/8 in. SS, 60/80 mesh). Reaction data were taken after 12 h of testing. The production rate of methanol is expressed in moles of methanol produced per kilogram Cu of the catalyst per hour. To obtain turnover frequency (TOF) for methanol formation, steady-state experiments were also conducted approximately at 5% CO_2

dx.doi.org/10.1021/cs300008g | ACS Catal. 2012, 2, 1667−1676

conversion to exclude the effect of water inhibition by increasing the WHSV up to 0.12 $m^3/g_{cat}/h$. TOF is defined as the number of methanol molecules produced per surface copper atoms of the reduced catalyst per second.

RESULTS AND DISCUSSION

1.0. Catalyst Characterization. *1.1. Reducibility.* The TPR profiles of pure CuO as a reference material and various Cu-based catalysts are displayed in Figure 1. Under the

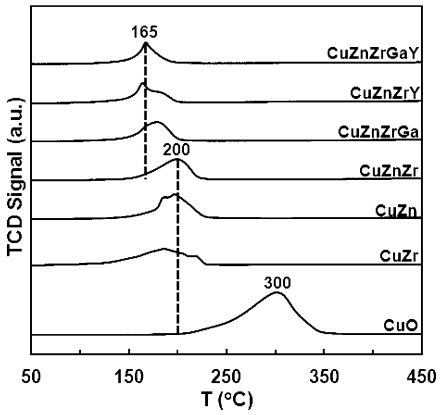

Figure 1. TPR profiles of the calcined catalysts.

experimental conditions used in this study, all metal oxides except CuO in these catalysts are nonreducible. The amount of H_2 consumption normalized to the Cu content is between 0.96 and 1.18, which is close to the stoichiometric value for CuO reduction ($CuO + H_2 \rightarrow Cu + H_2O$). The excess amount of H_2 consumption could be due to the reduction of hydroxycarbonate species left after air calcination at 350 °C.[46] All the TPR profiles exhibit one prominent reduction feature with some of the samples exhibiting structure within this feature. Generally, this feature and structure within it are assigned to the reduction of CuO to metallic Cu.[47,48] The structure within the TPR peak suggests that there are multiple types of CuO species with slight differences in ease of reducibility for the samples displaying this property. The low-temperature shoulder seen for the CuZn and CuZr catalysts has been ascribed to the reduction of amorphous or well-dispersed surface CuO species.[13,43,46,49] The shoulder may also originate from the stepwise reduction of CuO species via Cu_2O to Cu metal.[44,50] The addition of ZnO and ZrO_2 facilitates CuO reducibility as demonstrated by a shift of the peak maximum for the CuZr, CuZn, and CuZnZr catalysts to a lower temperature in comparison to bulk CuO. The incorporation of Ga_2O_3 and/or Y_2O_3 into the CuZnZr catalyst formulation further improves CuO reducibility as indicated by a shift of the TPR peak for the CuZnZrGa, CuZnZrY, and CuZnZrGaY samples. Moreover, the reduction feature of the CuZnZrGaY catalyst is symmetrical implying that CuO crystallites are homogeneously distributed.

1.2. Crystallinity. The XRD patterns of the catalysts calcined ex situ at 350 °C are shown in Figure 2a. For the CuZr catalyst, sharp diffraction peaks at 35.4° and 38.8° are characteristic of crystalline CuO with a monoclinic structure whereas a broad peak around 32° is associated with amorphous ZrO_2. This finding agrees well with the literature as crystalline zirconia phases were observed in the catalysts that were calcined above 500 °C.[47,51,52] The CuZn and CuZnZr catalysts show some crystallinity for both CuO and ZnO. When either Ga_2O_3 or

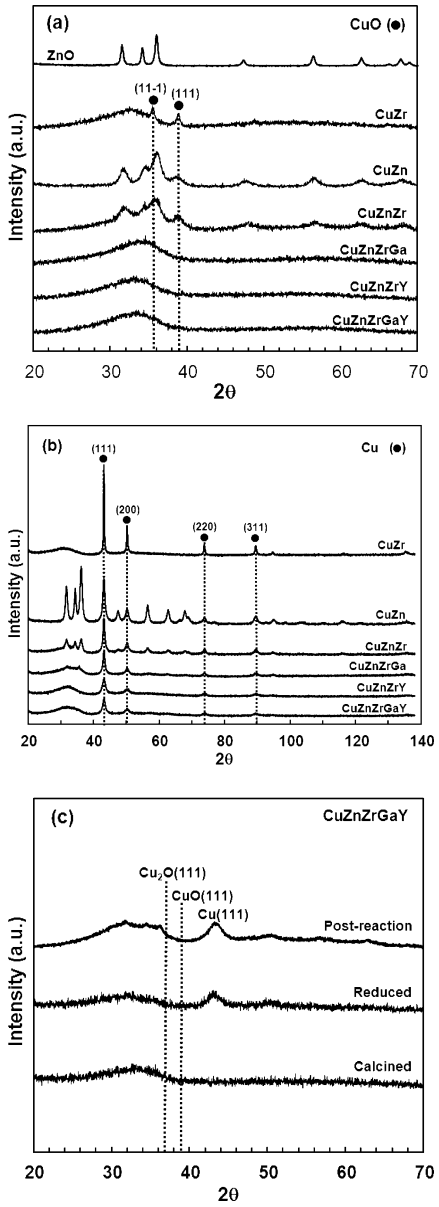

Figure 2. XRD patterns: (a) calcined catalysts, (b) reduced catalysts, and (c) CuZnZrGaY catalyst after subjecting to three different treatments.

Y_2O_3 is added to the CuZnZr catalyst formulation, the CuO and ZnO diffraction peaks disappear completely indicating that these metal oxides hinder the formation of larger XRD-detectable CuO and ZnO crystallites during calcination. Moreover, we do not see diffraction peaks for crystalline Ga- and Y-containing phases because they are either amorphous or highly dispersed in the catalysts.

Following in situ reduction at 250 °C, all bulk crystalline copper is in the metallic phase as confirmed by the appearance of the (111), (200), (220), and (311) peaks at 43.1°, 50.1°, 73.7°, and 89.3° respectively (Figure 2b). The CuZr catalyst exhibits the sharpest Cu diffraction peaks, suggesting that the Cu crystallite size of this catalyst is largest compared to those in the other catalysts. The bulk structure of copper in the spent CuZnZrGaY catalyst was further examined to demonstrate if the catalyst structure could be expected to change during 12-h reaction at 240 °C and 20 bar. As displayed in Figure 2c, copper

dx.doi.org/10.1021/cs300008g | ACS Catal. 2012, 2, 1667−1676

remains in the crystalline metallic phase under reaction conditions as the XRD pattern of the spent catalyst is similar to that collected with the reduced catalyst. The bulk oxidation of metallic Cu does not occur because we do not see XRD peaks for $Cu_2O(111)$ or $CuO(111)$ upon exposure to the feed gas. Additionally, bulk ZnO becomes slightly crystalline whereas other metal oxides (ZrO_2, Ga_2O_3, and Y_2O_3) in the spent catalyst remain amorphous or well-dispersed throughout the reaction.

Refinements of the in situ XRD patterns in Figure 2b were done using the pseudo-Voigt function (PVF) to determine the average Cu crystallite size and microstrain of the reduced catalysts. The PVF, which is the weighted sum of the Gaussian and Lorentzian contributions, allows us to model the overall line broadening with respect to both size and strain effects.[53] The best fits were obtained when both size and strain were refined together. Cu metal was the only refined crystalline component and the amorphous region from 25° to 35° was excluded from refinements (See Supporting Information). Rietveld analysis confirms that the average copper crystallite size is as small as 9 nm and decreases in the following order: CuZr ≫ CuZn > CuZnZr > CuZnZrGa > CuZnZrY > CuZnZrGaY. The XRD-determined crystallite sizes are very close to those obtained from the N_2O decomposition method except for the reduced CuZr sample (Figure 3). The average Cu crystallite size of this catalyst is likely to be the bulk value (i.e., larger than 40 μm) and is excluded from comparison.

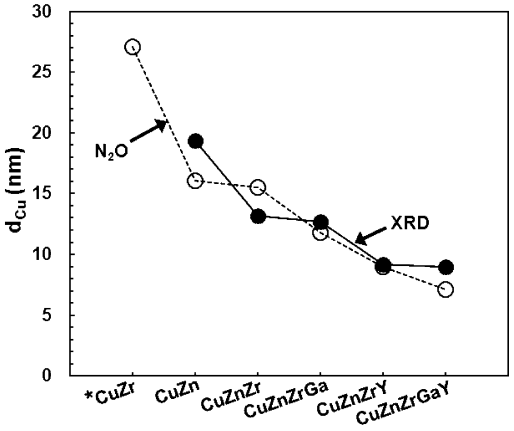

Figure 3. Comparison of copper crystallite sizes determined from Rietveld refinements and the N_2O decomposition method. *The XRD copper crystallite size of the reduced CuZr catalyst is not shown.

1.3. Morphology. TEM was conducted on the CuZn and CuZnZrGaY catalysts collected from the XRD sample holder after reduction at 250 °C to obtain insight into the morphology and crystallite size. As shown in Figure 4a, the reduced CuZn catalyst consists of particles with spherical and faceted shapes, and the majority of them aggregate to form irregularly shaped large clusters over 20 nm. In contrast, particles in the CuZnZrGaY catalyst are spherical and uniformly distributed (Figure 4b). The average diameter of the particles in the CuZnZrGaY catalyst is much smaller (~5−10 nm). The corresponding selected area electron diffraction (SAED) patterns display a series of concentric rings, which are indexed as face-centered cubic (fcc) Cu and wurtzite ZnO. Broad, diffuse rings without visible diffraction spots can be generated either by amorphous or very fine grained crystallites. The lack of visible spots in the SAED pattern of the reduced

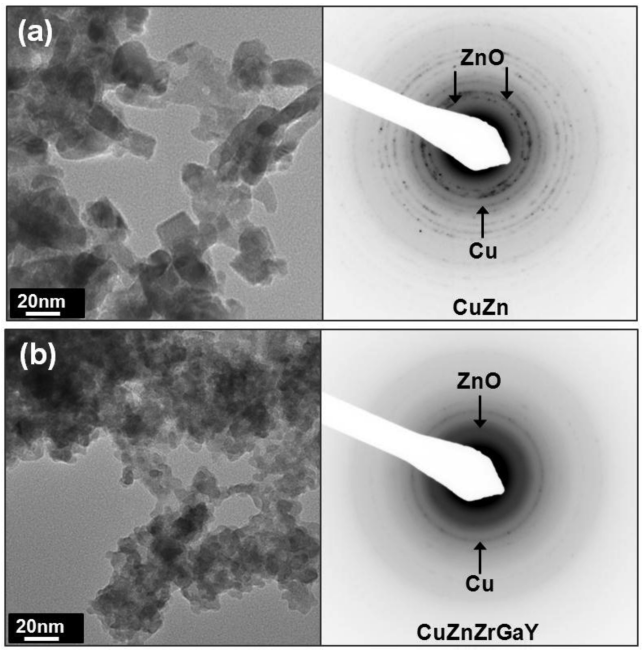

Figure 4. TEM images of the reduced catalysts collected after in situ XRD reduction and their corresponding electron diffraction patterns: (a) CuZn and (b) CuZnZrGaY.

CuZnZrGaY catalyst suggests that the grain size is much finer than that of the reduced CuZn catalyst if the crystalline phase is present. The TEM observations are consistent with the findings from TPR and in situ XRD. All copper species in the catalysts are reduced to metallic Cu after reduction at 250 °C. Because of the formation of highly dispersed CuO crystallites, the catalyst containing Ga_2O_3 and Y_2O_3 requires a lower temperature than the binary and ternary catalysts for complete reduction.

2.0. Chemical State of Copper Species. XPS analysis was performed to identify the oxidation state of copper species on the catalyst surface after three different treatments (e.g., calcination, reduction, reaction). The true chemical state of Cu-based active sites for methanol synthesis remains an unresolved issue in the literature with activity attributed to both Cu^0 and Cu^+ species.[34,54−60] Developing general insight into which Cu state is responsible for activity is important for engineering these systems for improved performance and gaining a fundamental understanding of their activity. The XPS data for all samples are nearly identical, so the spectra of the CuZnZrGaY catalyst are shown in Figure 5a as a representative result. XPS results for the other samples are included in the Supporting Information.

For the calcined sample, the Cu $2p_{3/2}$ and Cu $2p_{1/2}$ peaks are accompanied by prominent shakeup satellite features at 942 and 962 eV. These satellites are caused by the charge transfer between the transition metal 3d and surrounding ligand oxygen 2p orbitals and they do not appear in Cu_2O and Cu metal because their 3d orbitals are completely filled.[61−64] The Cu $2p_{3/2}$ peak BE of 933.8 eV is therefore indicative of Cu^{2+} species.[47,61,65−68] After reduction, the Cu $2p_{3/2}$ peak becomes much sharper and shifts to a lower binding energy at 931.7 eV. The disappearance of the satellite peaks verifies that there are no Cu^{2+} species left on the surface after reduction.[61,66,69] This observation is consistent with TPR results since the reduction of CuO in all the catalysts is completed well before 250 °C,

dx.doi.org/10.1021/cs300008g | ACS Catal. 2012, 2, 1667−1676

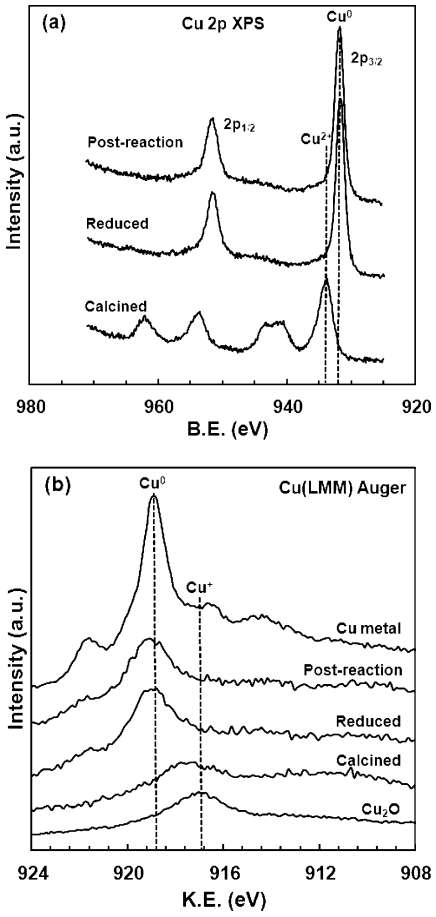

Figure 5. Spectra for the CuZnZrGaY catalyst after different treatments: (a) Cu 2p XPS and (b) Cu(LMM) Auger. Spectra for reference Cu metal and Cu_2O are included for comparison.

which is the reduction temperature used in this study (Figure 1). Further exposure to 25% CO_2/H_2 at 240 °C and ambient pressure for 8 h does not cause any noticeable change in the spectrum (Figure 5a).

It is difficult to differentiate between Cu^0 and Cu^+ species based on their Cu 2p binding energies, which are nearly identical. The Cu $2p_{3/2}$ BE is 932.2 eV for Cu_2O and is 932.4 eV for Cu metal.[70] As such, the kinetic energies of the Cu (LMM) Auger peaks are traditionally used to distinguish Cu^0 from Cu^+ species. The line position in the Cu (LMM) Auger spectrum of the CuZnZrGaY catalyst demonstrates that Cu^0 is the predominant copper species detectable on the surface of the reduced catalyst (Figure 5b). The Auger spectra of reference Cu_2O and Cu metal are also displayed in the same figure for comparison. After exposure to methanol synthesis conditions, the surface Cu species remain in the metallic state without being reoxidized to Cu^+ species. Overall, the Auger spectra of the reduced and reacted catalysts are very similar to that for metallic Cu. That similarity is based on the observed kinetic energy of the main peak and the presence of a weak shoulder on the higher kinetic energy side of the main peak for both catalysts and reference Cu metal foil. The Auger spectra of the reduced and reacted catalysts do not contain a shoulder on the lower kinetic energy side of their main peak, which would be indicative of a contribution from Cu^+ species. However, the background in the Auger spectra of the catalysts is higher than expected at lower kinetic energies because of overlap with the Auger peaks of Zn. These results are in agreement with Melian-Cabrera et al.,[64] Kilo et al.,[71] and Dai et al.[72] Most importantly, the XPS and Auger results illustrate that Cu^0 is the predominant copper species detectable in these samples after reduction and reaction and that Cu^+ species cannot be responsible for the activity of these catalysts.

CO_2+H_2-TPReaction was performed to obtain supporting evidence that the working catalysts were characterized by XPS. Over the representative CuZnZrGaY catalyst, the methanol signal begins to rise approximately at 180 °C, reaches a maximum around 230 °C, and then decreases at higher temperatures (Figure 6). Meanwhile, the CO_2 intensity

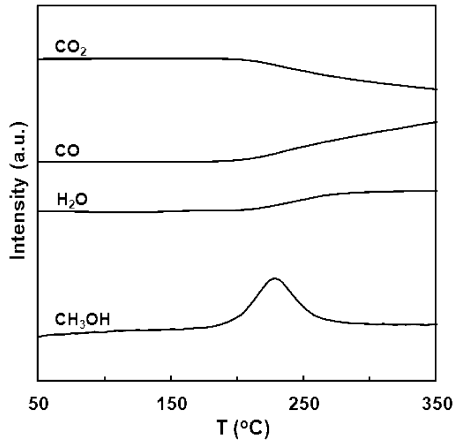

Figure 6. Profiles of products observed during CO_2+H_2-TPReaction of the CuZnZrGaY catalyst at atmospheric pressure.

decreases concurrently and continues to drop until the final temperature reaches 350 °C. Other reaction products such as CO and H_2O were also generated during the temperature ramp. The CO and H_2O signals keep rising above 200 °C as the endothermic reverse water-gas shift reaction ($CO_2 + H_2 \rightarrow CO + H_2O$) becomes favorable at higher temperatures. This experiment demonstrates that CO_2 is catalytically hydrogenated to methanol, which is detectable by a mass spectrometer even at atmospheric pressure. It is likely that the amount of any surface Cu^+ species, which could be produced from the oxidation of Cu metal by a low concentration of water vapor, is not appreciable enough to be detected by XPS-Auger. The presence of Cu_2O was detected in the bulk and on the surface of Cu/ZnO catalysts when wet syngas (i.e., 9 mol % H_2O) was fed to produce methanol.[73] It is worth noting that the equilibrium water content in the product stream is much lower than the amount of water in the feed gas used in the study of Wang et al.:[73] 3.8 mol % at 1 bar and 4.7 mol % at 20 bar based on the calculations using 1 mol of CO_2 and 3 mol of H_2 at 240 °C. Therefore, the surface copper species of the working catalysts remain in the metallic state under the experimental conditions used in this study as indicated by the KE values and shapes of the Cu(LMM) Auger peaks. Additional XPS data including a table of Cu $2p_{3/2}$ binding and Cu (LMM) kinetic energies and values of the modified Auger parameter are provided in the Supporting Information.

3.0. Correlations between Activity and Structural Parameters. To establish structure−activity relationships, the catalysts were evaluated for methanol synthesis at 240 °C and 20 bar. The steady-state activity is expressed with respect to the production rate of methanol after 12-h testing. It is evident that

dx.doi.org/10.1021/cs300008g | ACS Catal. 2012, 2, 1667−1676

the activity and Cu surface area are strongly correlated (Figure 7). In other words, catalysts with large Cu surface area exhibit

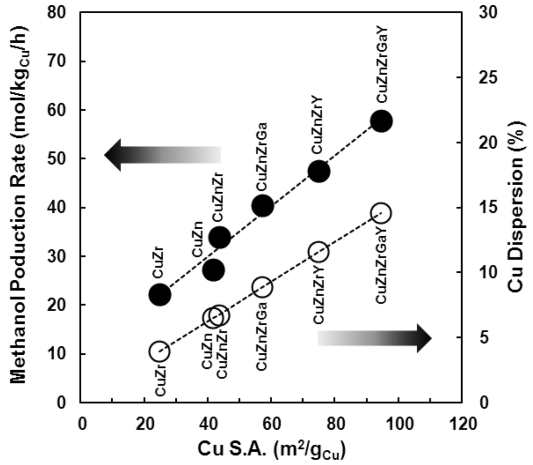

Figure 7. Methanol production rate and copper dispersion as a function of copper surface area for the reduced catalysts. Reaction conditions: 240 °C, 20 bar, $CO_2/H_2/N_2$ = 1/3/0.4, WHSV = 0.03 $m^3/g_{cat}/h$.

high rates of methanol production. As plotted in the same figure, Cu dispersion expectedly increases with Cu surface area because the metal dispersion is inversely proportional to the radius of the spherical particle.[74] The best-performing catalyst in the series, CuZnZrGaY, has the largest Cu surface area (94.4 m^2/g_{Cu}) and highest Cu dispersion (14.6%). Other researchers have observed a similar linear correlation between activity and copper surface area with catalysts supported on different metal oxides.[20−24]

The dependence of the turnover frequency (TOF) for methanol formation on Cu crystallite size is illustrated in Figure 8. High TOF values are achieved with small Cu crystallites, which is consistent with the trend based on the methanol production rates in Figure 7. Our TOF values are comparable to those from previously published studies under similar reaction conditions: ∼0.003−0.018 s^{-1} at 220−240 °C and 10−80 bar.[6,10,75] As a rule, a horizontal line in the plot of TOF vs

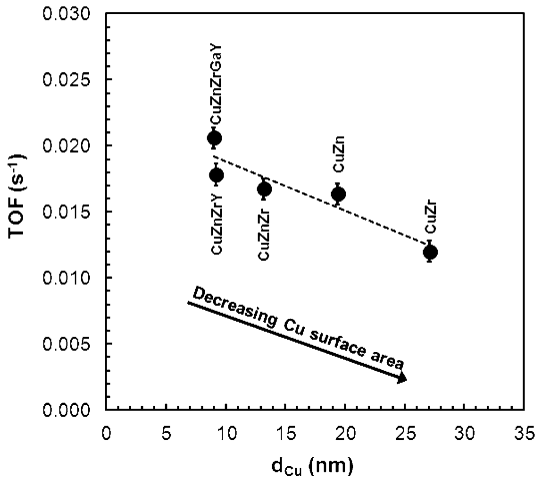

Figure 8. Relationship between TOF for methanol synthesis and copper crystallite size. Reaction conditions: 240 °C, 20 bar, $CO_2/H_2/N_2$ = 1/3/0.4, CO_2 conversion ≈5%.

crystallite size (or active surface area) is indicative of a structure-insensitive reaction.[13,45] Therefore, methanol synthesis via CO_2 hydrogenation is structurally sensitive because TOF decreases with increasing Cu crystallite size.

Generally, particle size can influence the proportions of low-index (111) and (100) planes, corner, and edge atoms, which in turn affect both surface structure and electronic properties.[76] Surfaces of larger particles primarily expose low-index facets, with fewer edge or defect sites.[77] In contrast, smaller crystallites have larger numbers of open planes, edge/defect sites containing coordinately unsaturated atoms which are typically more reactive than fully coordinated species. Experimental studies have been conducted mostly on model catalysts to demonstrate the structure sensitivity of CO_2 hydrogenation to methanol on Cu. Nakamura et al. reported that TOF at 250 °C on Zn-free single-crystal Cu surfaces decreased in the following order: (110) > (311) > (100) > (111).[78] Moreover, the activity of Zn-deposited Cu(111) was found to be 13-fold more active than Zn-free Cu(111) signifying the synergistic effect with the ZnO support. The activity was found to be proportional to the formate coverage (θ_{HCOO}) on the postreaction surfaces. Likewise, Yang et al. discovered that Cu nanoparticles supported on a ZnO(0001) single crystal exhibited higher activity than the Cu(111) planar surface upon exposure to a feed gas containing 0.5 atm of CO_2 and 4.5 atm of H_2 at 500−600 K.[79] The authors suggested that an improvement in the activity was associated with the presence of low-coordinated Cu sites in the nanoparticles, which stabilized key intermediates (i.e., HCOO, H_2COO, H_2CO, and H_3CO) and lowered the reaction barrier of the rate-limiting H_2COO hydrogenation. On the theoretical side, Hu et al. conducted an ab initio density functional theory (DFT) cluster study to establish the structure sensitivity of formate adsorption on Cu planes.[80] Calculations indicated that the adsorption energy decreased in the following order: (110) > (100) > (111), which is consistent with the activity trend experimentally observed by Nakamura et al.[78] Open Cu(110) or (100) facets or even step and defect sites are more reactive for catalyzing methanol synthesis from CO and CO_2 than close-packed Cu(111).[60,81] Additionally, a decline in the activity was accompanied by an increase in the Cu coordination number, which is indicative of Cu sintering.[82,83] More recently, experimental and computational studies on Cu/ZnO/Al_2O_3 catalysts have illustrated that Cu steps, stabilized by stacking faults or twin boundaries, increase the activity by stabilizing reaction intermediates and lowering activation barriers.[31] Our results showing higher activity with smaller Cu particles (Figure 8) are therefore consistent with all of these experimental and computational literature results on single-crystal surfaces, model catalysts, and heterogeneous catalysts. The large compositional changes in the catalysts presented in our work illustrate that the trend seen with Cu particle size is somewhat general and is not specific to a particular composition or model catalyst system.

Smaller Cu particles will also lead to larger interfacial area with the metal oxide support, suggesting that synergistic interactions with the support may also play a role in activity. The synergistic role of the ZnO support has been debated in the literature.[26,32,33,84−86] Unfortunately, our current experiments do not allow us to easily and directly probe this synergism. For the systems evaluated here, the content of ZnO and its crystallinity change dramatically. Despite these changes, the activity trend in Figure 8 still maps smoothly with Cu particle size, pointing to this as a predominant contributing

dx.doi.org/10.1021/cs300008g | ACS Catal. 2012, 2, 1667−1676

factor to activity. Other literature reports have found that Cu catalysts supported on other metal oxides (e.g., Al_2O_3, SiO_2, TiO_2, ZrO_2) are also capable of converting CO_2 to methanol without the presence of ZnO although these systems typically have lower activities than ZnO-based catalysts,[15,87] suggesting that the role of ZnO cannot be completely ruled out. Recent in situ XPS and computational studies have pointed to the role of $Zn^{\delta+}$ species at Cu steps/defects in increasing the binding strength of intermediates and decreasing reaction barriers.[31] This finding is consistent with our results illustrating the enabling role that small Cu particles in close contact with the Zn-containing mixed metal oxide support have on the activity. Furthermore, the trend seen across a range of catalyst compositions in this study demonstrates that Cu particle size, the presence of defects, and support interactions seem to be the important factors dictating the activity of these catalysts.[31] Future work will be conducted to gain a better understanding of the role of support, specifically the oxides of Ga, Zr, and Y, on the performance of Cu-based methanol synthesis catalysts.

Microstrain in copper crystallites is an additional structural parameter that has been suggested to influence the activity of Cu-based catalysts for methanol synthesis, the steam reforming of methanol, and low-temperature water-gas shift reaction.[39,40,88−92] Optimal catalysts were found to have large Cu microstrain, which in turn enhanced their performance in such reactions. Cu microstrain in Cu/ZnO catalysts was proposed to result from the following phenomena: (i) a certain fraction of ZnO dissolving in the bulk of the Cu phase, (ii) incomplete reduction of CuO, and (iii) epitaxial bonding of the ZnO lattice to Cu.[39] Catalyst composition, the type of precipitating agent, and aging time are key synthesis variables that can modify the interfacial contact between Cu and the oxide components. In the systems evaluated here, we find no correlation between TOF and Cu microstrain values obtained from Rietveld refinements (Figure 9). The addition of Ga_2O_3 and Y_2O_3 in the CuZnZr catalyst formulation does not appreciably affect the degree of strain detectable in the Cu crystallites. These results in Figures 8 and 9 indicate that Cu surface area is the predominant structural parameter that controls the activity whereas Cu microstrain is not generally responsible for the activity of these catalysts.

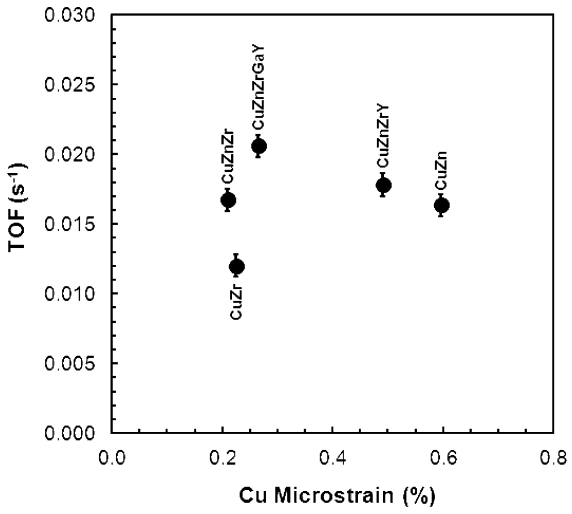

Figure 9. Variation of TOF with copper microstrain of the reduced catalysts.

CONCLUSIONS

Characterization of Cu-based catalysts prepared by reverse co-precipitation under ultrasonic treatment indicates that Cu^0 species are active sites for methanol synthesis from a stoichiometric mixture of CO_2 and H_2. Upon exposure to H_2/inert at 250 °C, CuO is fully reduced and all copper remains in the metallic phase after reaction. The possibility of Cu^+ species acting as active sites is excluded because these species are not observed on the surface of the working catalysts. Methanol synthesis from CO_2 is a structure-sensitive reaction with smaller Cu particles demonstrating higher TOF values. Although we find that the activity and Cu surface area are strongly correlated, a relationship between TOF and Cu microstrain cannot be established. The incorporation of Ga_2O_3 and Y_2O_3 into CuZnZr catalysts enhances the Cu dispersion and reducibility, thus giving rise to superior methanol synthesis activity.

ASSOCIATED CONTENT

Supporting Information

Detailed procedure for refinements of XRD patterns collected after in situ reduction. A table displaying refined and derived parameters determined by Rietveld refinements for all catalysts. A table summarizing Cu $2p_{3/2}$ binding and Cu (LMM) kinetic energies and values of the modified Auger parameter for all 6 catalysts after being subject to different treatments. Additional corresponding Cu 2p XPS and Cu(LMM) Auger spectra. This material is available free of charge via the Internet at http://pubs.acs.org.

AUTHOR INFORMATION

Corresponding Author

*E-mail: Sittichai.Natesakhawat@NETL.DOE.GOV. Phone: (412) 386-5096. Fax: (412) 386-5920.

Funding

As part of the National Energy Technology Laboratory's Regional University Alliance (NETL-RUA), a collaborative initiative of the NETL, this technical effort was performed under the RES contract DE-FE-0004000. This project was funded by the Department of Energy, National Energy Technology Laboratory, an agency of the United States Government, through a support contract with URS Energy & Construction, Inc. Neither the United States Government nor any agency thereof, nor any of their employees, nor URS Energy & Construction, Inc., nor any of their employees, makes any warranty, expressed or implied, or assumes any legal liability or responsibility for the accuracy, completeness, or usefulness of any information, apparatus, product, or process disclosed, or represents that its use would not infringe privately owned rights. Reference herein to any specific commercial product, process, or service by trade name, trademark, manufacturer, or otherwise, does not necessarily constitute or imply its endorsement, recommendation, or favoring by the United States Government or any agency thereof. The views and opinions of authors expressed herein do not necessarily state or reflect those of the United States Government or any agency thereof.

Notes

The authors declare no competing financial interest.

REFERENCES

(1) Centi, G.; Perathoner, S. *Catal. Today* **2009**, *148*, 191−205.

(2) Olah, G. A.; Goeppert, A.; Prakash, G. K. S. *J. Org. Chem.* **2009**, *74*, 487−498.
(3) Bartholomew, C. H.; Farrauto, R. J. In *Fundamentals of Industrial Catalytic Processes*, 2nd ed.; John Wiley & Sons, Inc.: Hoboken, NJ, 2006; pp 83−391.
(4) Ma, Y.; Sun, Q.; Wu, D.; Fan, W. H.; Zhang, Y. L.; Deng, J. F. *Appl. Catal., A* **1998**, *171*, 45−55.
(5) Sloczynski, J.; Grabowski, R.; Kozlowska, A.; Olszewski, P.; Lachowska, M.; Skrzypek, J.; Stoch, J. *Appl. Catal., A* **2003**, *249*, 129−138.
(6) Sloczynski, J.; Grabowski, R.; Kozlowska, A.; Olszewski, P.; Stoch, J.; Skrzypek, J.; Lachowska, M. *Appl. Catal., A* **2004**, *278*, 11−23.
(7) Sloczynski, J.; Grabowski, R.; Olszewski, P.; Kozlowska, A.; Stoch, J.; Lachowska, M.; Skrzypek, J. *Appl. Catal., A* **2006**, *310*, 127−137.
(8) Yang, C.; Ma, Z.; Zhao, N.; Wei, W.; Hu, T.; Sun, Y. *Catal. Today* **2006**, *115*, 222−227.
(9) Raudaskoski, R.; Niemela, M. V.; Keiski, R. L. *Top. Catal.* **2007**, *45*, 57−60.
(10) Arena, F.; Barbera, K.; Italiano, G.; Bonura, G.; Spadaro, L.; Frusteri, F. *J. Catal.* **2007**, *249*, 185−194.
(11) Arena, F.; Italiano, G.; Barbera, K.; Bordiga, S.; Bonura, G.; Spadaro, L.; Frusteri, F. *Appl. Catal., A* **2008**, *350*, 16−23.
(12) Arena, F.; Italiano, G.; Barbera, K.; Bonura, G.; Spadaro, L.; Frusteri, F. *Catal. Today* **2009**, *143*, 80−85.
(13) Guo, X.; Mao, D.; Lu, G.; Wang, S.; Wu, G. *J. Catal.* **2010**, *271*, 178−185.
(14) Inui, T.; Hara, H.; Takeguchi, T.; Kim, J. B. *Catal. Today* **1997**, *36*, 25−32.
(15) Saito, M. *Catal. Surv. Jpn.* **1998**, *2*, 175−184.
(16) Toyir, J.; Piscina, P.R.d.l.; Fierro, J. L. G.; Homs, N. *Appl. Catal., B* **2001**, *29*, 207−215.
(17) Toyir, J.; Piscina, P.R.d.l.; Fierro, J. L. G.; Homs, N. *Appl. Catal., B* **2001**, *34*, 255−266.
(18) Toyir, J.; Piscina, P.R.d.l.; Llorca, J.; Fierro, J. L. G.; Homs, N. *Phys. Chem. Chem. Phys.* **2001**, *3*, 4837−4842.
(19) Clancy, P.; Breen, J. P.; Ross, J. R. H. *Catal. Today* **2007**, *127*, 291−294.
(20) Chinchen, G. C.; Waugh, K. C.; Whan, D. A. *Appl. Catal.* **1986**, *25*, 101−107.
(21) Pan, W. X.; Cao, R.; Roberts, D. L.; Griffin, G. L. *J. Catal.* **1988**, *114*, 440−446.
(22) Robbins, J. L.; Iglesia, E.; Kelkar, C. P.; DeRites, B. *Catal. Lett.* **1991**, *10*, 1−10.
(23) Burch, R.; Golunski, S. E.; Spencer, M. S. *Catal. Lett.* **1990**, *5*, 55−60.
(24) Baltes, C.; Vukojevic, S.; Schuth, D. *J. Catal.* **2008**, *258*, 334−344.
(25) Koeppel, R. A.; Baiker, A. *Appl. Catal., A* **1992**, *84*, 77−102.
(26) Kurtz, M.; Bauer, N.; Buscher, C.; Wilmer, H.; Hinrichsen, O.; Becker, R.; Rabe, S.; Merz, K.; Driess, M.; Fischer, R. A.; Muhler, M. *Catal. Lett.* **2004**, *92*, 49−52.
(27) Saito, M.; Fujitani, T.; Takeuchi, M.; Watanabe, T. *Appl. Catal., A* **1996**, *138*, 311−318.
(28) Nakamura, J.; Nakamura, I.; Uchijima, T.; Kanai, Y.; Watanabe, T.; Saito, M.; Fujitani, T. *J. Catal.* **1996**, *160*, 65−75.
(29) Herman, R. G.; Klier, K.; Simmons, G. W.; Finn, B. P.; Bulko, J. B.; Kobylinski, T. P. *J. Catal.* **1979**, *56*, 407−429.
(30) Mehta, S.; Simmons, G. W.; Klier, K.; Herman, R. G. *J. Catal.* **1979**, *57*, 339−360.
(31) Behrens, M.; Studt, F.; Kasatkin, I.; Kuhl, S.; Havecker, M.; Abild-Pedersen, F.; Zander, S.; Girgsdies, F.; Kurr, P.; Kniep, B. L.; Tovar, M.; Fischer, R. W.; Norskov, J. W.; Schlogl, R. *Science* **2012**, *336*, 893−897.
(32) Fujitani, T.; Nakamura, J. *Catal. Lett.* **1998**, *56*, 119−124.
(33) Fujitani, T.; Nakamura, J. *Appl. Catal., A* **2000**, *191*, 111−129.
(34) Choi, Y.; Futagami, K.; Fujitani, T.; Nakamura, J. *Catal. Lett.* **2001**, *73*, 27−31.
(35) Millar, G. J.; Rochester, C. H.; Waugh, K. C. *J. Chem. Soc., Faraday Trans.* **1992**, *88*, 3497−3503.
(36) Bussche, K. M. V.; Froment, G. F. *Appl. Catal., A* **1994**, *112*, 37−55.
(37) Bailie, J. E.; Rochester, C. H.; Millar, G. J. *Catal. Lett.* **1995**, *31*, 333−340.
(38) Poels, E. K.; Brands, D. S. *Appl. Catal., A* **2000**, *191*, 83−96.
(39) Gunter, M. M.; Ressler, T.; Bems, B.; Buscher, C.; Genger, T.; Hinrichsen, O.; Muhler, M.; Schlogl, R. *Catal. Lett.* **2001**, *71*, 37−44.
(40) Kasatkin, I.; Kurr, P.; Kniep, N.; Trunschke, A.; Schlogl, R. *Angew. Chem., Int. Ed.* **2007**, *46*, 7324−7327.
(41) Jung, K. T.; Bell, A. T. *Catal. Lett.* **2002**, *80*, 63−68.
(42) Khassin, A. A.; Pelipenko, V. V.; Minyukova, T. P.; Zaikovskii, V. I.; Kochubey, D. I.; Yurieva, T. M. *Catal. Today* **2006**, *112*, 143−147.
(43) Chary, K. V. R.; Sagar, G. V.; Srikanth, C. S.; Rao, V. V. *J. Phys. Chem. B* **2007**, *111*, 543−550.
(44) Balaraju, M.; Rekha, V.; Prasad, P. S. S.; Prasad, R. B. N.; Lingaiah, N. *Catal. Lett.* **2008**, *126*, 119−124.
(45) Satterfield, C. N. In *Heterogeneous Catalysis in Industrial Practice*, 2nd ed.; Krieger Publishing Company: Malabar, FL, 1996; pp 15−179.
(46) Breen, J. P.; Ross, J. R. H. *Catal. Today* **1999**, *51*, 521−533.
(47) Matter, P. H.; Braden, D. J.; Ozkan, U. S. *J. Catal.* **2004**, *223*, 340−351.
(48) Gawade, P.; Mirkelamoglu, B.; Ozkan, U. S. *J. Phys. Chem. C* **2010**, *114*, 18173−18181.
(49) Chary, K. V. R.; Sagar, G. V.; Naresh, D.; Seela, K. K.; Sridhar, B. *J. Phys. Chem. B* **2005**, *109*, 9437−9444.
(50) Jones, S. D.; Hagelin-Weaver, H. E. *Appl. Catal., B* **2009**, *90*, 195−204.
(51) Labaki, M.; Lamonier, J. F.; Siffert, S.; Zhilinskaya, E. A.; Aboukais, A. *Colloids Surf., A* **2003**, *227*, 63−75.
(52) Esposito, S.; Turco, M.; Bagnasco, G.; Cammarano, C.; Pernice, P.; Aronne, A. *Appl. Catal., A* **2010**, *372*, 48−57.
(53) McCusker, L. B.; Dreele, R. B. V.; Cox, D. E.; Louer, D.; Scardi, P. *J. Appl. Crystallogr.* **1999**, *32*, 36−50.
(54) Liu, X. M.; Lu, G. Q.; Yan, Z. F.; Beltramini, J. *Ind. Eng. Chem. Res.* **2003**, *42*, 6518−6530.
(55) Okamoto, Y.; Fukino, K.; Imanaka, T.; Teranishi, S. *J. Phys. Chem.* **1983**, *87*, 3747−3754.
(56) Kuznetsov, B. N.; Chudinov, M. G.; Alekseev, A. M.; Yakerson, V. I. *Kinet. Catal.* **1995**, *36*, 539−543.
(57) Harikumar, K. R.; Rao, C. N. R. *Appl. Surf. Sci.* **1998**, *125*, 245−249.
(58) Peplinski, B.; Unger, W. E. S.; Grohmann, I. *Appl. Surf. Sci.* **1992**, *62*, 115−129.
(59) Apai, G. R.; Monnier, J. R.; Hanrahan, M. J. *J. Chem. Soc., Chem. Commun.* **1984**, 212−213.
(60) Yoshihara, J.; Campbell, C. T. *J. Catal.* **1996**, *161*, 776−782.
(61) Jones, S. D.; Neal, L. M.; Hagelin-Weaver, H. E. *Appl. Catal., B* **2008**, *84*, 631−642.
(62) Campos-Martin, J. M.; Guerrero-Ruiz, A.; Fierro, J. L. G. *J. Catal.* **1995**, *156*, 208−218.
(63) Fleisch, T. H.; Mieville, R. L. *J. Catal.* **1984**, *90*, 165−172.
(64) Melian-Cabrera, I.; Granados, M. L.; Terreros, P.; Fierro, J. L. G. *Catal. Today* **1998**, *45*, 251−256.
(65) Wang, L. C.; Liu, Y. M.; Chen, M.; Cao, Y.; He, H. Y.; Wu, G. S.; Dai, W. L.; Fan, K. N. *J. Catal.* **2007**, *246*, 193−204.
(66) Rodriguez-Ramos, I.; Guerrero-Ruiz, A.; Rojas, M. L.; Fierro, J. L. G. *Appl. Catal.* **1991**, *68*, 217−228.
(67) Siriwardane, R. V.; Poston, J. A. *Appl. Surf. Sci.* **1993**, *68*, 65−80.
(68) Goodby, B. E.; Pemberton, J. E. *Appl. Spectrosc.* **1988**, *42*, 754−760.
(69) Ono, Y.; Wakita, H.; Inui, T. *Catal. Lett.* **1998**, *53*, 83−89.
(70) Wagner, C. D.; Riggs, W. M.; Davis, L. E.; Moulder, J. F. In *Handbook of X-Ray Photoelectron Spectroscopy*; Muilenberg, G.E., Ed.; Perkin-Elmer Corporation: Eden Prairie, MN, 1979; p 171.
(71) Kilo, M.; Weigel, J.; Wokaun, A.; Koeppel, R. A.; Stoeckli, A.; Baiker, A. *J. Mol. Catal. A* **1997**, *126*, 169−184.
(72) Dai, W. L.; Sun, Q.; Deng, J. F.; Wu, D.; Sun, Y. H. *Appl. Surf. Sci.* **2001**, *177*, 172−179.

(73) Wang, D.; Han, Y.; Tan, Y.; Tsubaki, N. *Fuel Process. Technol.* **2009**, *90*, 446−451.
(74) Kolasinski, K. W. In *Surface Science: Foundations of Catalysis and Nanoscience*, 2nd ed.; John Wiley & Sons Ltd.: Chichester, England, 2008; p 296.
(75) Sun, Q.; Zhang, Y.-L.; Chen, H.-Y.; Deng, J.-F.; Wu, D.; Chen, S.-Y. *J. Catal.* **1997**, *167*, 92−105.
(76) Uzio, D.; Berhault, G. *Catal. Rev.* **2010**, *52*, 106−131.
(77) Rioux, R. M.; Song, H.; Hoefelmeyer, J. D.; Yang, P.; Somorjai, G. A. *J. Phys. Chem. B* **2005**, *109*, 2192−2202.
(78) Nakamura, I.; Fujitani, T.; Uchijima, T.; Nakamura, J. *J. Sci. Technol. A* **1996**, *14*, 1464−1468.
(79) Yang, Y.; Evans, J.; Rodriguez, J. A.; White, M. G.; Liu, P. *Phys. Chem. Chem. Phys.* **2010**, *12*, 9909−9917.
(80) Hu, Z.; Boyd, R. J. *J. Chem. Phys.* **2000**, *112*, 9562−9568.
(81) Grabow, L. C.; Mavrikakis, M. *ACS Catal.* **2011**, *1*, 365−384.
(82) Clausen, B. S.; Schiotz, J.; Grabaek, L.; Ovesen, C. V.; Jacobsen, K. W.; Norskov, J. K.; Topsoe, H. *Top. Catal.* **1994**, *1*, 367−376.
(83) Grunwaldt, J. D.; Molenbroek, A. M.; Topsoe, N. Y.; Topsoe, H.; Clausen, B. S. *J. Catal.* **2000**, *194*, 452−460.
(84) Chen, H. Y.; Lau, S. P.; Chen, L.; Lin, J.; Huan, C. H. A.; Tan, K. L.; Pan, J. S. *Appl. Surf. Sci.* **1999**, *152*, 193−199.
(85) Choi, Y.; Futagami, K.; Fujitani, T.; Nakamura, J. *Appl. Catal., A* **2001**, *208*, 163−167.
(86) Nakamura, J.; Uchijima, T.; Kanai, Y.; Fujitani, T. *Catal. Today* **1996**, *28*, 223−230.
(87) Saito, M.; Wu, J.; Tomoda, K.; Takahara, I.; Murata, K. *Catal. Lett.* **2002**, *83*, 1−4.
(88) Kniep, B. L.; Girgsdies, F.; Ressler, T. *J. Catal.* **2005**, *236*, 34−44.
(89) Muhamad, E. N.; Irmawati, R.; Taufiq-Yap, Y. H.; Abdullah, A. H.; Kniep, B. L.; Girgsdies, F.; Ressler, T. *Catal. Today* **2008**, *131*, 118−124.
(90) Li, L.; Song, L.; Wang, H.; Chen, C.; She, Y.; Zhan, Y.; Lin, X.; Zheng, Q. *Int. J. Hydrogen Energy* **2011**, *36*, 8839−8849.
(91) Ressler, T.; Kniep, B. L.; Kasatkin, I.; Schlogl, R. *Angew. Chem., Int. Ed.* **2005**, *44*, 4704−4707.
(92) Kurr, P.; Kasatkin, I.; Girgsdies, F.; Trunschke, A.; Schlögl, R.; Ressler, T. *Appl. Catal., A* **2008**, *348*, 153−164.